

# Chameleonic Photo- and Mechanoluminescence in Pyrazolate-Bridged NHC Cyclometalated Platinum Complexes

*Violeta Sicilia,\* Lorenzo Arnal, Daniel Escudero,\* Sara Fuertes\* and Antonio Martin*

## ABSTRACT

DFT investigations on the ground (GS) and the first triplet ( $T_1$ ) excited state potential energy surfaces (PES) were performed on a new series of platinum-butterfly complexes,  $[\{Pt(C^*C^*)(\mu-Rpz)\}_2]$  (Rpz: pz **1**, 4-Mepz **2**, 3,5-dmpz **3**, 3,5-dppz **4**) containing a cyclometalated NHC in their wings. The geometries of two close-lying local minima corresponding to butterfly-spread conformers, **1s-4s** and butterfly-folded ones, **1f-4f** with long and short Pt-Pt separations respectively were optimized in the GS and  $T_1$  PES. A comparison of the GS and  $T_1$  energy profiles revealed that an opposite trend is obtained in the relative stability of folded and spread conformers, being the latter more stabilized in their GS. Small  $\Delta G$  (s/f) along with small-energy barriers in the GS supports the co-existence of both kinds of conformers, which influence the photo- and mechanoluminescence of these complexes. In 5% wt doped PMMA films in the air, these complexes exhibit intense sky-blue emissions (PLQY: 72.0 % - 85.9%) upon excitation at  $\lambda \leq 380$  nm arising from  $^3IL/MLCT$  excited states, corresponding to the predominant **1s-4s** conformers. Upon excitation at longer wavelengths (up to 450 nm), the minor **1f-4f** conformers afford a blue emission as well, with PLQY still significant (40%-60%). In the solid state, the as-prepared powder of **4** exhibits a greenish-blue emission with QY  $\sim 29\%$ , mainly due to  $^3IL/MLCT$  excited states of butterfly-spread molecules, **4s**. Mechanical grinding resulted in an

enhanced and yellowish-green emission (QY ~ 51%) due to the <sup>3</sup>MMLCT excited states of butterfly-folded molecules, **4f**, in such a way that the mechanoluminescence has been associated with an intramolecular structural change induced by mechanical grinding.

## INTRODUCTION

Cyclometalated complexes of Pt(II) are characterized by outstanding photoluminescent properties,<sup>1</sup> arising from the radiative deactivation of triplet excited states, and which are at the origin of many challenging applications such as optical sensors,<sup>2</sup> biological imaging<sup>3</sup> or light emitting devices.<sup>4</sup> The planar geometry of the mononuclear complexes allows them to assemble through Pt...Pt and  $\pi$ - $\pi$  interactions. Recent computational investigations demonstrate that mononuclear complexes often possess very different photophysical properties than their aggregates. Thus, while mononuclear complexes are likely to deactivate nonradiatively through triplet metal-centered (<sup>3</sup>MC) excited states<sup>5</sup> the formation of the latter states is likely more hindered in condensed phases. Additionally, it was found that the formation of excimers in Pt(II) complexes is more favored than the formation of ground state aggregates.<sup>6</sup> As a result, the nature of the emissive triplet state changes from a monomer-based triplet emission to a triplet metal-metal-to-ligand charge transfer (<sup>3</sup>MMLCT) like-emission in the molecular ensembles, leading to red-shifted emissions.<sup>7, 8</sup> This kind of platinum compounds very often suffer the so-called aggregation-cause quenching (ACQ)<sup>9</sup> effect, which limits their applications. However, many transition metal complexes exhibit aggregation-induced phosphorescent emission (AIPE)<sup>10-14</sup> and they can successfully be used to achieve white light<sup>15, 16</sup> or NIR<sup>17, 18</sup> organic-light-emitting diodes by adjusting the doping concentration. The emission colour strongly depends on the extend of these intermolecular interactions, and in its turn, on environmental factors able to affect them, such as temperature variations,<sup>8</sup> mechanical force,<sup>12, 19</sup> or volatile solvent molecules embedded

into the lattice.<sup>2, 20</sup> Thus, these compounds become thermo-, mechano- and/or vapoluminescent complexes, enlarging the technological interest of these smart functional materials.

Compared to mononuclear complexes, binuclear luminescent complexes have been less explored.<sup>21-28</sup> In binuclear Pt(II) cyclometalated compounds, the metallophilic interactions and thereto their luminescent properties can partially be controlled by selecting the bridging ligands, which result in different degrees of rigidity and steric hindrance.<sup>21, 23, 24</sup> Among them, platinum complexes with bridging pyrazolates have been deeply studied by Castellano,<sup>25</sup> Thompson,<sup>26, 27</sup> and Ma<sup>28</sup> and coworkers. It was found that the Pt-Pt distance and the extent of the metallophilic interactions can be tuned by the bulkiness of the pyrazolate unit (butterfly body), in such a way that when the bulkiness increases the cycloplatinated units (butterfly wings) are pushed closer together. As a result, the emission colour of this kind of complexes can be tuned from blue to green or red.<sup>23</sup> Besides, in solution they exhibit sometimes a photoinduced structural change (PSC) on the lowest triplet-state potential energy surface (PES), resulting in a dramatic change of the Pt-Pt bond distance and thereto on the emission.<sup>28</sup> This unique butterfly-like structure allows the contraction of the Pt-Pt distance with temperature, and thus leading to solid-state thermochromism and thermoluminescence. This is the case of  $[\{\text{Pt}(\text{ppy})(\mu\text{-Ph}_2\text{pz})\}_2]$ ,<sup>29</sup> which at low temperature exhibits monomer-based <sup>3</sup>LC/MLCT emission and it changes to excimer-like <sup>3</sup>MMLCT emission above 160 K.

The cyclometalating groups play also an important role in the stability and the control of the photophysical properties.<sup>30</sup> In this sense, the platinum-butterfly complexes reported by Strassner et al., i.e.,  $[\{\text{Pt}(\text{C}^{\wedge}\text{C}^*)(\mu\text{-Rpz})\}_2]$ <sup>31, 32</sup> are exemplary ones. They revealed that the cyclometalated N-heterocyclic carbenes (C<sup>∧</sup>C\*), forming two strong metal-carbon bonds, are excellent wings for the synthesis of highly efficient blue and orange emitters. In this field, we reported compound

$[\{\text{Pt}(\text{C}^{\wedge}\text{C}^*)(\mu\text{-pz})\}_2]$  ( $\text{HC}^{\wedge}\text{C}^* = 1\text{-}(4\text{-}(\text{ethoxy-carbonyl})\text{phenyl})\text{-}3\text{-methyl-}1\text{H-imidazol-}2\text{-ylidene}$ ; pz: pyrazolate **1**) which undergoes two-centers, two-electron [2c, 2e] oxidation in the presence of haloforms ( $\text{CHX}_3$ , X= Cl, Br, I).<sup>33</sup> Herein we report three new complexes,  $[\{\text{Pt}(\text{C}^{\wedge}\text{C}^*)(\mu\text{-Rpz})\}_2]$  (Rpz: 4-methylpyrazolate (4-Mepz) **2**; 3,5-dimethylpyrazolate (3,5-dmpz) **3**; and 3,5-diphenylpyrazolate (3,5-dppz) **4**) bearing the same wings,  $\text{C}^{\wedge}\text{C}^*$ , but different bodies (Rpz). Besides the experimental synthesis and characterization of compounds **1-4**, the intriguing luminescence and mechanoluminescence have been studied and deciphered with Density Functional Theory (DFT) and time-dependent DFT (TD-DFT) investigations. For all the complexes two close-lying local minima corresponding to the folded (**f**) and spread (**s**) conformers were located on both the ground-state (GS) and the lowest adiabatic triplet excited state ( $T_1$ ) PES. Low energy barrier for the thermal interconversion between both structures in the GS seems to be at the core of the stimuli-responsive luminescence of complex **4** in the solid state.

## EXPERIMENTAL SECTION

Compounds  $[\{\text{Pt}(\text{EtO}_2\text{C-C}^{\wedge}\text{C}^*)(\mu\text{-Cl})\}_2]$  (**A**),<sup>34</sup>  $[\text{Pt}(\text{EtO}_2\text{C-C}^{\wedge}\text{C}^*)(4\text{-MepzH})_2]\text{ClO}_4$  (**B2**)<sup>35</sup> and  $[\{\text{Pt}(\text{EtO}_2\text{C-C}^{\wedge}\text{C}^*)(\mu\text{-pz})\}_2]$  (**1**)<sup>36</sup> were prepared as described elsewhere.

**Synthesis of *syn-/anti-*  $[\{\text{Pt}(\text{EtO}_2\text{C-C}^{\wedge}\text{C}^*)(\mu\text{-4-Mepz})\}_2]$  (**2**).**  $\text{NEt}_3$  (0.5 mL, 3.62 mmol) was added to a solution of **B2** (133.5 mg, 0.19 mmol) in acetone (30 mL) at rt. After 2 h of reaction the solvent was removed in vacuo to 2 mL. The solution was treated with  $\text{H}_2\text{O}$  (20 mL), filtered, and washed with  $\text{H}_2\text{O}$  to give **2-anti** (**83 %**)/ **2-syn** (**17%**) as a yellow solid. Yield: 73.7 mg, 75 %. Anal.Calcd for  $\text{C}_{34}\text{H}_{36}\text{N}_8\text{O}_4\text{Pt}_2$ : C, 40.40; H, 3.59; N, 11.08. Found: C, 40.00; H, 3.75; N, 11.06.  $^1\text{H}$  NMR data for **2-anti** (500 MHz, acetone- $d_6$ ):  $\delta = 8.02$  (d,  $^4J_{\text{H}_7, \text{H}_9} = 1.8$ ,  $^3J_{\text{H}_7, \text{Pt}} = 55.1$ , 2H,  $\text{H}_7$ ), 7.65 (d,  $^3J_{\text{H}_2, \text{H}_3} = 2.1$ , 2H,  $\text{H}_2$ ), 7.63 (dd,  $^3J_{\text{H}_9, \text{H}_{10}} = 8.1$ ,  $^4J_{\text{H}_9, \text{H}_7} = 1.8$ , 2H,  $\text{H}_9$ ), 7.50 (s, 2H,  $\text{H}_{3'}$ , 4-

Mepz), 7.46 (s, 2H, H<sub>5</sub>, 4-Mepz), 7.18 (d, <sup>3</sup>J<sub>H<sub>10</sub>, H<sub>9</sub></sub> = 8.1, 2H, H<sub>10</sub>), 7.06 (d, <sup>3</sup>J<sub>H<sub>3</sub>, H<sub>2</sub></sub> = 2.1, 2H, H<sub>3</sub>), 4.23 (m, CH<sub>2</sub>, CO<sub>2</sub>Et), 3.35 (s, 6H, H<sub>4</sub>), 2.12 (s, 6H, Me, 4-Mepz), 1.31 (t, <sup>3</sup>J<sub>H, H</sub> = 7.1, 6H, CH<sub>3</sub>, CO<sub>2</sub>Et). <sup>1</sup>H NMR data for **2-syn**: δ = 7.97 (d, <sup>4</sup>J<sub>H<sub>7</sub>, H<sub>9</sub></sub> = 1.8, 2H, H<sub>7</sub>), 7.68 (d, <sup>3</sup>J<sub>H<sub>2</sub>, H<sub>3</sub></sub> = 2.1, 2H, H<sub>2</sub>), 7.58 (dd, <sup>3</sup>J<sub>H<sub>9</sub>, H<sub>10</sub></sub> = 8.1, <sup>4</sup>J<sub>H<sub>9</sub>, H<sub>7</sub></sub> = 1.8, 2H, H<sub>9</sub>), 7.54 (s, 2H, H<sub>3</sub>, 4-Mepz), 7.42 (s, 2H, H<sub>5</sub>, 4-Mepz), 3.63 (s, 6H, H<sub>4</sub>), 1.35 (t, <sup>3</sup>J<sub>H, H</sub> = 7.1, 6H, CH<sub>3</sub>, CO<sub>2</sub>Et) the rest of the signals appear overlapped with those of the **2-anti** isomer. <sup>13</sup>C{<sup>1</sup>H} NMR plus HSQC and HMBC data for **2-anti** (125.75 MHz, acetone-*d*<sub>6</sub>): δ = 161.2 (C<sub>1</sub>), 152.9 (C<sub>5</sub>), 139.6 and 138.3 (C<sub>3</sub> and C<sub>5</sub>), 136.3 (C<sub>7</sub>), 133.8 and 126.8 (C<sub>6</sub> and C<sub>8</sub>), 126.3 (C<sub>9</sub>), 123.3 (C<sub>3</sub>), 116.2 (C<sub>2</sub>), 116.1 (C<sub>4</sub>), 110.9 (C<sub>10</sub>), 60.7 (CH<sub>2</sub>, CO<sub>2</sub>Et), 36.5 (C<sub>4</sub>), 14.6 (CH<sub>3</sub>, CO<sub>2</sub>Et), 9.5 (Me, 4-Mepz). <sup>13</sup>C{<sup>1</sup>H} NMR plus HSQC and HMBC data for **2-syn** (125.75 MHz, acetone-*d*<sub>6</sub>): δ = 160.3 (C<sub>1</sub>), 123.1 (C<sub>3</sub>), 36.7 (C<sub>4</sub>). <sup>195</sup>Pt{<sup>1</sup>H} NMR (108 MHz, acetone-*d*<sub>6</sub>): δ = -3775 (**2-anti**), -3785 (**2-syn**) ppm. (MS (MALDI+): m/z 1010.4 [Pt(C<sup>^</sup>C\*)(μ-4-Mepz)}<sub>2</sub>].

**Synthesis of syn-/anti- [Pt(EtO<sub>2</sub>C-C<sup>^</sup>C\*)(μ-3,5-dmpz)}<sub>2</sub>] (**3**).** Compound **A** (106.3 mg, 0.12 mmol) was added to a solution containing NaO<sup>t</sup>Bu (22.2 mg, 0.23 mmol) and 3,5-dmpzH (22.5 mg, 0.23 mmol) in acetone/EtOH (10 mL /5 mL). After 3 h of reaction at -10°C, the solvent was removed to 3 mL under reduced pressure, filtered and washed with 2 x 5 mL of H<sub>2</sub>O to give **3-anti** (**80 %**)/ **3-syn** (**20%**) as a yellow solid. Yield: 70 mg, 58 %. Anal. Calcd for C<sub>36</sub>H<sub>40</sub>N<sub>8</sub>O<sub>4</sub>Pt<sub>2</sub>: C, 41.62; H, 3.88; N, 10.79. Found: C, 41.24; H, 4.02; N, 10.76. <sup>1</sup>H NMR data for **3-anti** (500 MHz, methylene chloride- *d*<sub>2</sub>): δ = 7.83 (d, <sup>4</sup>J<sub>H<sub>7</sub>, H<sub>9</sub></sub> = 1.7, <sup>3</sup>J<sub>H<sub>7</sub>, Pt</sub> = 52.3, 2H, H<sub>7</sub>), 7.67 (d, <sup>3</sup>J<sub>H<sub>9</sub>, H<sub>10</sub></sub> = 7.5, 2H, H<sub>9</sub>), 7.20 (s, br, 2H, H<sub>2</sub>), 6.94 (d, <sup>3</sup>J<sub>H<sub>10</sub>, H<sub>9</sub></sub> = 7.5, 2H, H<sub>10</sub>), 6.67 (s, br, 2H, H<sub>3</sub>), 6.11 (s, 2H, H<sub>4</sub>, dmpz), 4.24 (m, CH<sub>2</sub>, CO<sub>2</sub>Et), 3.33 (s, 6H, H<sub>4</sub>), 2.32 and 2.27 (s, 12H, Me, dmpz), 1.35 (t, <sup>3</sup>J<sub>H, H</sub> = 7.1, 6H, CH<sub>3</sub>, CO<sub>2</sub>Et). <sup>1</sup>H NMR data for **3-syn**: δ = 6.13 and 6.04 (s, 2H, H<sub>4</sub>, dmpz), 3.58 (s, 6H, H<sub>4</sub>), the rest of the signals appear overlapped with those of the **3-anti**.

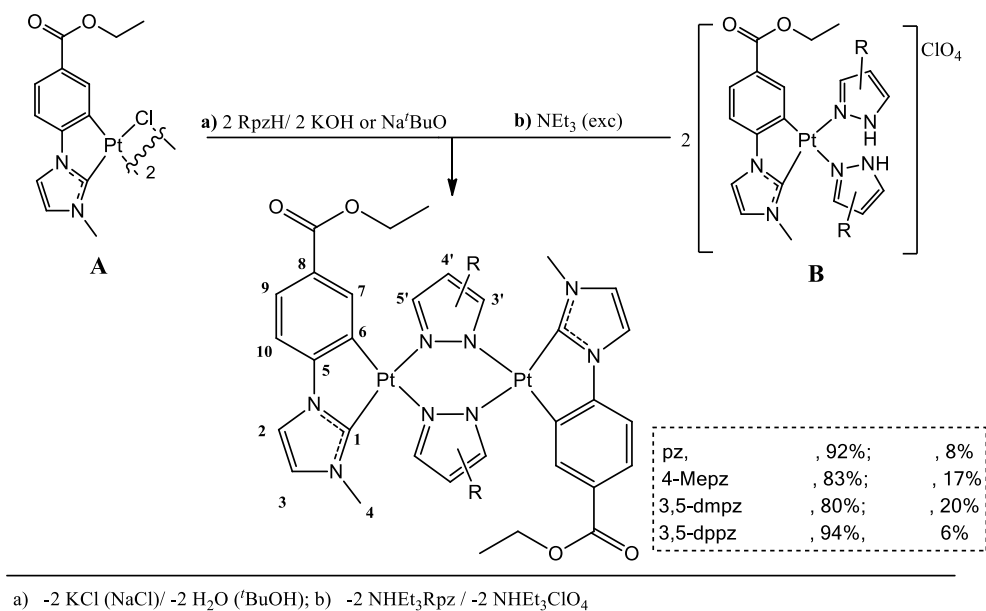
$^{13}\text{C}\{^1\text{H}\}$  NMR plus HSQC and HMBC data for **3-anti** (125.75 MHz, methylene chloride- $d_2$ ):  $\delta$  = 160.7 ( $\text{C}_1$ ), 152.2 ( $\text{C}_5$ ), 146.7 ( $\text{C}_3$ , and  $\text{C}_5$ ), 136.9 ( $\text{C}_7$ ), 133.4 and 126.7 ( $\text{C}_6$  and  $\text{C}_8$ ), 125.9 ( $\text{C}_9$ ), 122.1 ( $\text{C}_3$ ), 115.4 ( $\text{C}_2$ ), 110.2 ( $\text{C}_{10}$ ), 104.6 ( $\text{C}_4$ ), 60.8 ( $\text{CH}_2$ ,  $\text{CO}_2\text{Et}$ ), 35.7 ( $\text{C}_4$ ), 14.7 ( $\text{CH}_3$ ,  $\text{CO}_2\text{Et}$ ), 14.2 (Me, dmpz).  $^{13}\text{C}\{^1\text{H}\}$  NMR plus HSQC and HMBC data for **3-syn** (125.75 MHz, methylene chloride- $d_2$ ): 160.2 ( $\text{C}_1$ ), 35.8 ( $\text{C}_4$ ).  $^{195}\text{Pt}\{^1\text{H}\}$  NMR (108 MHz, methylene chloride-  $d_2$ ):  $\delta$  = -3771 ppm (**3-anti**), -3799 (**3-syn**) ppm. MS (MALDI+): m/z 1038.2 [ $\{\text{Pt}(\text{C}^{\wedge}\text{C}^*) (\mu\text{-dmpz})\}_2$ ].

**Synthesis of syn-/anti- [ $\{\text{Pt}(\text{EtO}_2\text{C-C}^{\wedge}\text{C}^*) (\mu\text{-3,5-dppz})\}_2$ ] (**4**).**  $\text{AgClO}_4$  (52.7 mg, 0.25 mmol) was added to a stirred suspension of **A** (115.8 mg, 0.12 mmol) in acetone (30 mL) in the dark at room temperature. After 2 h of reaction, 3,5-dppzH (110.9 mg, 0.50 mmol) was added to the mixture and allowed to react overnight in the darkness. Then, the resulting suspension was filtered through Celite and concentrated to ca. 20 mL.  $\text{NEt}_3$  (0.5 mL, 3.62 mmol) was added to the reaction mixture and stirred for 2 h. Then, the solvent was removed in vacuo. The residue was treated with cold MeOH (5 mL) and filtered to give **4-anti** (**94%**)/ **4-syn** (**6%**) as a yellow solid. Yield: 90.0 mg, 74 %. Anal. Calcd for  $\text{C}_{56}\text{H}_{48}\text{N}_8\text{O}_4\text{Pt}_2$ : C, 52.25; H, 3.76; N, 8.71. Found: C, 52.64; H, 3.90; N, 8.82.  $^1\text{H}$  NMR data for **4-anti** (500 MHz,  $\text{DMSO-}d_6$ , 353K):  $\delta$  = 8.59 (d,  $^3J_{\text{H}_o, \text{H}_m} = 7.2$ , 4H,  $\text{H}_o$ ), 8.25 (dd,  $^3J_{\text{H}_o, \text{H}_m} = 7.2$ ,  $^4J_{\text{H}_o, \text{H}_p} = 1.8$ , 4H,  $\text{H}_o$ ), 7.84 (s, br, 1H,  $\text{H}_{\text{C}^{\wedge}\text{C}^*}$ ), 7.72 – 7.53 (m, 4H,  $\text{H}_{\text{C}^{\wedge}\text{C}^*}$ ), 7.50 – 7.24 (m, 9H,  $\text{H}_{\text{pz}}$  and  $\text{H}_{\text{C}^{\wedge}\text{C}^*}$ ), 7.20 – 7.03 (m, 8H,  $\text{H}_{\text{pz}}$  and  $\text{H}_{\text{C}^{\wedge}\text{C}^*}$ ), 6.99 (s, br, 2H,  $\text{H}_{\text{pz}}$ ), 4.18 (q,  $^3J_{\text{H}, \text{H}} = 7.0$ , 4H,  $\text{CH}_2$ ,  $\text{CO}_2\text{Et}$ ), 3.18 (s, 6H,  $\text{H}_4$ ), 1.29 (t,  $^3J_{\text{H}, \text{H}} = 7.0$ , 6H,  $\text{CH}_3$ ,  $\text{CO}_2\text{Et}$ ).  $^1\text{H}$  NMR data for **4-syn**:  $\delta$  = 3.32 (s, 6H,  $\text{H}_4$ ), the rest of the signals appear overlapped with those of the **4-anti** isomer.  $^{13}\text{C}\{^1\text{H}\}$  NMR plus HSQC and HMBC data for **4-anti** (125.75 MHz,  $\text{DMSO-}d_2$ , 353K):  $\delta$  = 155.5 ( $\text{C}_1$ ), 135.1 ( $\text{C}_{\text{C}^{\wedge}\text{C}^*}$ ), 132.7 ( $\text{C}_{\text{pz}}$ ), 132.6 ( $\text{C}_{\text{pz}}$ ), 127.6 ( $\text{C}_{\text{pz}}$ ), 127.0 ( $\text{C}_{\text{pz}}$ ), 126.8 ( $\text{C}_{\text{C}^{\wedge}\text{C}^*}$ ), 126.7 ( $\text{C}_o$ ), 125.4 ( $\text{C}_o$ ), 124.7 ( $\text{C}_{\text{C}^{\wedge}\text{C}^*}$ ), 124.5 ( $\text{C}_{\text{C}^{\wedge}\text{C}^*}$ ), 122.1 ( $\text{C}_{\text{C}^{\wedge}\text{C}^*}$ ), 109.7 ( $\text{C}_{\text{C}^{\wedge}\text{C}^*}$ ), 103.2 ( $\text{C}_{\text{C}^{\wedge}\text{C}^*}$ ), 59.3 ( $\text{CH}_2$ ,  $\text{CO}_2\text{Et}$ ), 34.3 ( $\text{C}_4$ ), 13.6 ( $\text{CH}_3$ ,  $\text{CO}_2\text{Et}$ ).  $^{195}\text{Pt}\{^1\text{H}\}$  NMR (108

MHz, DMSO- $d_6$ , 353K):  $\delta = -3680$  ppm (**4-anti**). (MS (MALDI+):  $m/z$  1286.5 [ $\{\text{Pt}(\text{C}^*\text{C}^*)(\mu\text{-}3,5\text{-dppz})\}_2$ ].

## RESULTS AND DISCUSSION

Compounds [ $\{\text{Pt}(\text{C}^*\text{C}^*)(\mu\text{-Rpz})\}_2$ ] ( $\text{HC}^*\text{C}^* = 1\text{-}(4\text{-}(\text{ethoxycarbonyl})\text{ phenyl})\text{-}3\text{-methyl-}1H\text{-imidazol-}2\text{-ylidene}$ ; Rpz: 4-methylpyrazolate (4-Mepz) **2**; 3,5-dimethylpyrazolate (3,5-dmpz) **3**; 3,5-diphenylpyrazolate (3,5-dppz) **4**) were prepared following path a (for **3**) or b (for **2** and **4**) in Scheme 1.).



Scheme 1. Synthetic routes followed for compounds **1-4**. Just the major isomer “*anti*” appears represented for clarity along with its numerical scheme for NMR analysis. Compound **1** is included for overview.

The inability to get compound **3** through path b, is in agreement with the greater basicity of 3,5-dmpzH<sup>37</sup> with respect to pzH, 4-MepzH and 3,5-dppzH, which prevents it to be removed from the coordination sphere of the platinum center (experimental details for **2-4** in the SI). All the complexes were obtained as a mixture of *syn/anti* isomers with respect to the relative orientation of the cyclometalated C<sup>^</sup>C\* groups, with the anti-isomer being the predominant one, as it can be seen in the <sup>1</sup>H and the <sup>195</sup>Pt{<sup>1</sup>H} NMR spectra of **2-4** (Figures S1-S4). The single-crystal X-ray diffraction study of **2** and **3** confirmed the expected spread butterfly-like structure (Figure 1). Like compound **1**,<sup>36</sup> complex **2** showed three different molecules in the asymmetric unit (A, B, C) with intermetallic distances of 3.355(4) Å (**2A**), 3.224(3) Å (**2B**) and 3.156(3) Å (**2C**). However, complex **3** exhibited only one dinuclear molecule with an intermetallic separation of 3.131(17) Å, in the low range of distances observed in other platinum- butterfly complexes with the same body (3,5-dmpz) but bearing different wings (3.128-3.203 Å).<sup>26, 38-40</sup> Unfortunately, no good quality crystals were obtained for **4**, but we could confirm the atom connectivity. Two different molecules with Pt-Pt separation of 3.054 Å and 2.982 Å were found in the asymmetric unit. Therefore, once again it can be established that when the steric demand of the bridging pyrazolate increases the platinum centers are pushed closer together, like in other butterfly-like platinum complexes reported by Thompson,<sup>26</sup> Umakoshi<sup>40</sup> and Strassner.<sup>32</sup> An extended description of these molecules has been included in SI (see Table S2 and Figures S5- S7).

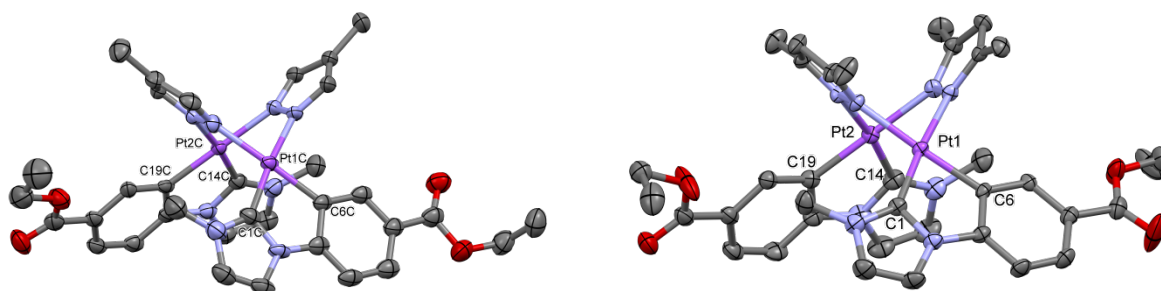




Figure 1. Molecular structures of **2A** (left) and **3** (right). Ellipsoids are drawn at their 50% probability level; solvent molecules and hydrogen atoms have been omitted for clarity.

**Theoretical calculations.** DFT calculations on the GS and the lowest adiabatic triplet excited state ( $T_1$ ) PESs for **1-4** were performed and the geometries of relevant stationary points, such as e.g., local minima and transition states (TS) were optimized (see SI for computational details) accounting for solvent effects in THF.

For all the complexes, the geometries of two close-lying local minima were optimized in the GS PES (see Figure S8 in SI) which corresponded to the butterfly-spread structures **1s-4s** and the butterfly-folded ones **1f-4f**. Those corresponding to the butterfly-spread conformers **1s-4s** show long Pt-Pt distances (3.10 Å for **4s**, 3.10 Å for **3s** < 3.20 Å for **1s** < 3.22 Å for **2s**) and intramolecular C<sup>^</sup>C\* separations (> 4.5 Å) following the same trend than the one observed in the experimental values. Also, they are characterized by a small Pt-Pt bond order (BO: 0.036 **4s** < 0.106 **3s** < 0.110 **1s** < 0.111 **2s**). On the other hand, the GS optimized geometries corresponding to the butterfly-folded conformers **1f-4f**, are characterized by shorter Pt-Pt distances (2.96 Å for **4f** < 2.97 Å for **3f**, 2.97 Å for **1f** < 2.98 Å for **2f**) and intramolecular C<sup>^</sup>C\* contacts (< 3.8 Å) along with larger Pt-Pt bond orders (BO: 0.170 **4f**, 0.174 **3f** < 0.228 **1f** < 0.233 **2f**) than those of **1s-4s**. The computed energy profiles in the GS PES are shown in Figure 2. For all compounds, the conformers **1s-4s**, featuring longer Pt-Pt distances, are more stable than the conformers **1f-4f** ( $\Delta G$ : 0.076 eV (1.76 kcal/mol) for **4**, 0.129 eV (2.97 kcal/mol) for **1**, 0.152 eV (3.50 kcal/mol) for **3**; and 0.220 eV (5.08 kcal/mol) for **2**). Especially, this is remarkable for **2s**, which bears the longest Pt-Pt separation and the largest dihedral angle between the two platinum coordination

planes. Besides, for complexes bearing bulkier Rpz units (**3** and **4**), their **3s** and **4s** minima are stabilized at shorter Pt-Pt distances than **1s** and **2s**.

Furthermore, for complexes **1** and **2**, we have successfully located the transition state (TS) associated with the interconversion between both conformers (see their optimized geometries in Figure S8). These TSs lie exemplarily 0.0077 eV (0.18 kcal/mol) above **1f**, and 0.037 eV (0.86 kcal/mol) above **2f** (see Figure 2). Their optimized geometries display Pt-Pt distances which lie in between those found for the butterfly-folded and butterfly-spread optimized minima. In the case of **1**,<sup>33</sup> a small  $\Delta G$  (**1s/1f**) value along with a small activation barrier supports, within the experimental error, a fast thermal equilibration in the ground state PES, thus resembling an intramolecular *butterfly flapping-like* motion.

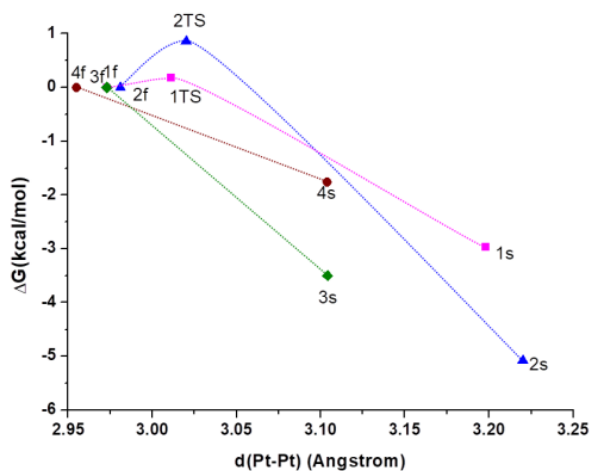


Figure 2: Calculated relative energy profile (PCM-M06/6-31G(d) and MWB60(Pt)) in the GS for the interconversion between the **1f-4f** and **1s-4s** conformers. Values calculated in THF.

These results are fully consistent with the presence of both conformers in solution, with the butterfly-spread being the predominant one. Attempts to optimize the geometries of the TSs for the interconversion between conformers of complexes **3-4** were unsuccessful. In view of this

piece of evidence, the flipping process likely occurs in a barrierless manner for the latter complexes.

Let us now discuss the results for the calculations on the lowest adiabatic triplet excited state ( $T_1$ ) PES. The geometries of two local minima i.e., **s/f**, were optimized for the all complexes (Figure 3, and Figure S9 in SI). The optimized geometries for the butterfly-spread conformers, **1s-4s**, show Pt-Pt distances ( $3.02 \text{ \AA}$  for **4s** <  $3.09 \text{ \AA}$  for **3s** <  $3.20 \text{ \AA}$  for **2s** <  $3.21 \text{ \AA}$  for **1s**) and Pt-Pt bond orders (BO: 0.116 **3s**, 0.110 **2s**, 0.102 **4s**, 0.099 **1s**), similar to those observed for most of them in the GS.

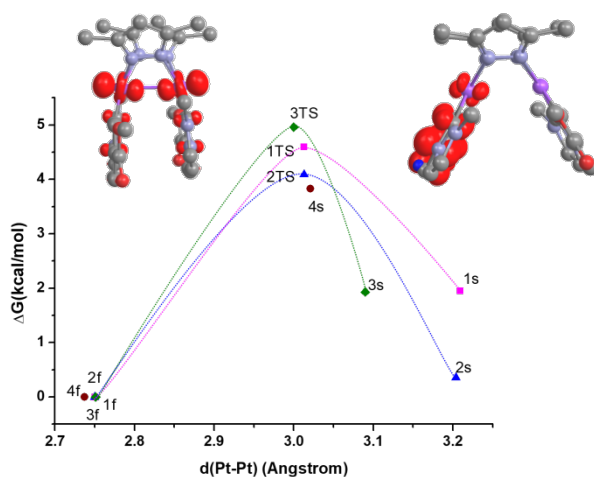


Figure 3: Calculated relative energy profile (PCM-M06/6-31G(d) and MWB60(Pt)) in the lowest adiabatic triplet excited state ( $T_1$ ) for the interconversion between the **1f-4f** and **1s-4s** conformers. Values calculated in THF. Spin density distribution plots of **3f** (left) and **3s** (right).

However, the  $T_1$  optimized geometries for the butterfly-folded conformers, **1f-4f**, exhibit intermetallic separations ( $2.74 \text{ \AA}$  for **4f** <  $2.75 \text{ \AA}$  for **1f-3f**), which are shortened by ca.  $0.22 \text{ \AA}$  with respect to those in the GS and Pt-Pt bond orders (BO: 0.586 **4f**, 0.591 **3f**, 0.626 **2f**, 0.621 **1f**)

which are increased by 0.4 with respect to those in the GS. The calculated spin density distribution for **1s-4s** indicates a mixed  ${}^3\text{IL}/{}^3\text{MLCT}$  [ $\pi(\text{C}^{\wedge}\text{C}^*) \rightarrow \pi^*(\text{C}^{\wedge}\text{C}^*)/5d(\text{Pt}) \rightarrow \pi^*(\text{C}^{\wedge}\text{C}^*)$ ] character for their  $T_1$  states (see Figure 3 and S10), while a  ${}^3\text{MMLCT}$  [ $d\sigma^*(\text{Pt-Pt}) \rightarrow \pi^*(\text{C}^{\wedge}\text{C}^*)$ ] character for the  $T_1$  states of **1f-4f**. Note that the changes in the Pt-Pt distances and the BO values from the GS to  $T_1$  states in the butterfly-folded conformers **1f-4f**, almost agree with a one-electron excitation from the  $d\sigma^*(\text{Pt-Pt})$  orbital.

Like in the previously reported C,N-cycloplatinated butterfly-like complexes by Ma et al.,<sup>28</sup> as the steric bulk of the Rpz ligand increases their spread-like minima ( ${}^3\text{IL}/{}^3\text{MLCT}$ ) display shorter Pt-Pt bond distances (compare e.g., **1s**, **2s** vs **3s** and **4s** in Figure 3). Importantly, comparing the **1s-4s** and the **1f-4f** optimized geometries in their  $T_1$  states, there is a considerable shortening of the Pt-Pt distances in the folded-like structures. The change of excited state character when going from the **1s-4s** minima ( ${}^3\text{IL}/{}^3\text{MLCT}$ ) to the **1f-4f** ones ( ${}^3\text{MMLCT}$ ) leads to an extra stabilization of the latter conformers<sup>41</sup> by 0.085 eV (1.95 kcal/mol), 0.015 eV (0.36 kcal/mol), 0.084 eV (1.93 kcal/mol) and 0.166 eV (3.83 kcal/mol) for complexes **1-4** respectively. Note also that certain amount of Pt-Pt bonding is only possible in the  $T_1$  state but not in the GS.

All in all, a comparison of the GS and  $T_1$  energy profiles reveals that an opposite trend is obtained in the relative stability of folded and spread conformers, being the former clearly more stabilized in their  $T_1$  states, regardless of the steric hindrance of the bridging Rpz, but specially for complex **4**. Besides, we located the transition states (TSs) for the interconversion between conformers in the  $T_1$  state for **1-3**, which are shown in Figure S9. These TSs all bear one imaginary frequency associated with the interconversion between both conformers. These TSs lie 0.115 eV (2.65 kcal/mol), 0.162 eV (3.73 kcal/mol) and 0.132 eV (3.04 kcal/mol) above the local

minima **1s-3s** respectively. These energy-barriers for PSC are larger than those for the flapping-like intramolecular motion in the GS

The absorption properties of **1-4** were also investigated with PCM-TD-DFT calculations in the presence of THF (see details in the SI). The results are collected in Tables S3, S4 and Figure S11. The frontier molecular orbitals (Figure S11) for **1s-4s** and **1f-4f** along with the energies of their lowest singlet excited states were also calculated (see inset of Figure 4 and Table S4 in SI). The lowest singlet excited states have predominant HOMO to LUMO character and can be described mainly as  $^1\text{MLCT}/^1\text{IL}$  [ $5d(\text{Pt}) \rightarrow \pi^*(\text{C}^{\wedge}\text{C}^*)$ ] / [ $\pi(\text{C}^{\wedge}\text{C}^*) \rightarrow \pi^*(\text{C}^{\wedge}\text{C}^*)$ ] for **1s-4s**, while some additional  $^1\text{MMLCT}$  [ $d\sigma^*(\text{Pt-Pt}) \rightarrow \pi^*(\text{C}^{\wedge}\text{C}^*)$ ] character is found for those of **1f-4f**. The vertical  $\Delta\text{SCF-M06}$  emission energies from the  $T_1$  optimized geometries were calculated as well, rendering values of ca. 510 nm for **1s-4s** and of ca. 570 nm for **1f-4f** (see Table S4 in SI).

**Photophysical properties.** The absorption and emission properties of **1-4** were investigated and explained on the basis of the DFT calculations. The UV-vis spectra of **1-4** (Figure 4 and Table S26 in SI) do not show differences between diluted ( $10^{-5}$  M) and concentrated solutions ( $10^{-3}$  M). They show their lowest-energy absorption bands ( $\epsilon \sim 9 \cdot 10^3 \text{ M}^{-1} \text{ cm}^{-1}$ ) in the range 325- 390 nm. These absorptions bands match the  $S_0 \rightarrow S_1$  transitions calculated for the butterfly-spread molecules **1s-4s** (see Figure 4), which are the predominant species according to the calculations.

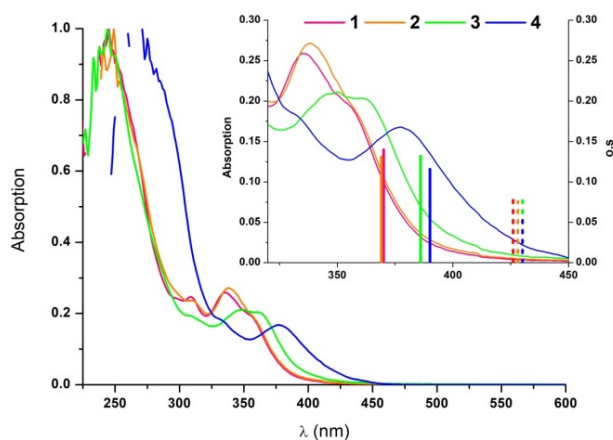


Figure 4: UV-visible spectra (pathlength: 1mm) of **1-3** in 2-MeTHF  $10^{-3}$  M and **4** in 2-MeTHF  $10^{-5}$ M (pathlength: 1cm). Inset: Expanded view of the UV-Vis spectra along with the TD-M06/6-31G(d) and MWB60(Pt)  $S_0 \rightarrow S_1$  transitions of the butterfly-spread (solid bars) and butterfly-folded (dashed bars) conformers.

However, in spite of the low contribution of the Rpz to the frontier molecular orbitals (FMOs) this absorption appears clearly red-shifted as the bulkiness of the R groups on the bridging pyrazolate increases. So, for species **3s** and **4s**, exhibiting shorter intermetallic distances and smaller interplanar angles in the GS, some  $^1\text{MMLCT}$  [ $d\sigma^*(\text{Pt-Pt}) \rightarrow \pi^*(\text{C}^{\wedge}\text{C}^*)$ ] character could be reasonably attributed (see Figure S8 and S11).

Diluted solutions ( $10^{-5}$  M) of **1-4** in 2-MeTHF were fast-cooled to 77K. Upon excitation at  $\lambda \leq 340$  nm, each of their emission spectra were characterized by a highly structured emission bands with  $\lambda_{\text{max}} \sim 450$  nm and vibronic spacings [ $\sim 1450 \text{ cm}^{-1}$ ], likely corresponding to the C=C / C=N bond stretching modes of the cyclometalated NHC ligands (Figure 5, left). The emission energies are not affected by the nature of the Rpz ligands and they are very similar to those observed in the mononuclear compounds bearing the same “(C $\wedge$ C\*)Pt” fragment.<sup>34, 35, 42, 43</sup>

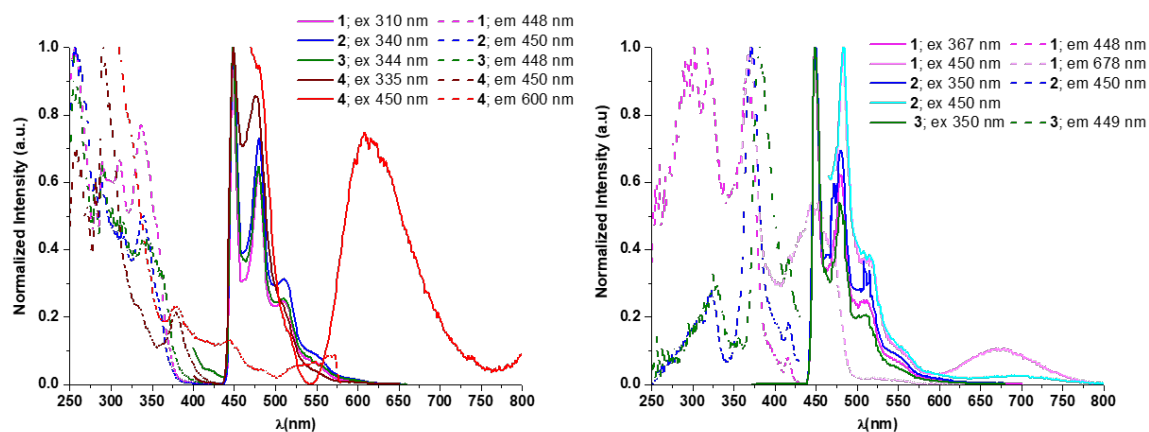


Figure 5. Normalized excitation (dotted lines) and emission (solid lines) spectra at 77K under Ar atmosphere, left: **1-4** in 2-MeTHF 10<sup>-5</sup>M; right: **1-3** in 2-MeTHF 10<sup>-3</sup>M

The computed emission energies for the butterfly-spread conformers, i.e., **1s-4s**, agree better with the experimental findings at 77 K than those calculated from **1f-4f**. Thus, these results highlight that the barriers for interconversion between **s/f** conformers at the T<sub>1</sub> state (see Figure 3) are large enough to prevent their thermal equilibrium at 77 K.

Complexes **1** and **4** show additional excitation and emission bands at lower energies ( $\lambda_{\text{exc}} \sim 450$  nm,  $\lambda_{\text{em}} > 600$  nm), attributable to the butterfly-folded molecules (calculated S<sub>1</sub>  $\sim$  426 nm; T<sub>1</sub> = 572 nm for **1f**; and S<sub>1</sub>  $\sim$  429 nm; T<sub>1</sub> = 570 nm for **4f**), although for **1** they are only perceptible in concentrated solutions (10<sup>-3</sup> M) (Figure 5 right). The coexistence of butterfly-spread and butterfly-folded molecules for **1** and **4**, is in accordance with the small  $\Delta G$  value computed between the two conformers, **s/f** in the ground state ( $\Delta G$ : 0.076 eV (1.76 kcal/mol) **4s/4f**, 0.129 eV (2.97 Kcal/mol) **1s/1f**) within the experimental error (MUE (M06) = 2.48 kcal/mol, see SI). For complexes **2** and **3** because of the greater  $\Delta G$  between them (0.220 eV (5.08 kcal/mol) **2s/2f**, 0.152 eV (3.50 Kcal/mol) **3s/3f**) it seems to be more unlikely and undetectable at 77K.

In 5% wt doped PMMA films in the air, excitation of complexes **1-4** at  $\lambda \leq 380$  nm affords intense sky-blue emissions with quantum yields of 72.0% **1**, 83.4% **2**, 79.0% **3** and 85.9% **4** (see Table 1). These emissions match with those observed in 2-MeTHF ( $10^{-5}$ M) at 77K. The slight blue-shift in the emission spectra upon cooling is in accordance with an emissive state of  $^3\text{IL}/^3\text{MLCT}$  character. The excitation of these films at longer wavelengths, up to 450 nm, render less intense but matched emission bands (see Figure 6; Table S27 and Figure S12 in SI). It should be noted the short radiative decay of these emissions at r. t., which are similar to those observed in analogous complexes  $[\{\text{Pt}(\text{C}^*\text{C}^*)(\mu\text{-Rpz})\}_2](\text{HC}^*\text{C}^* = 3\text{-dibenzofuran-4-yl-1-methyl-3H-imidazol-2-ylidene, imidazopyridine-2-ylidene; R = H, Me, tBu})$ ,<sup>31, 32</sup> but clearly shorter than those measured for mononuclear compounds containing the same “(C\* C\*)Pt” fragment.<sup>37, 38</sup>

All these pieces of evidence highlight a greater metallic contribution to the excited state and then, a greater  $^3\text{MLCT}$  character of the blue emissions of complexes **1-4** in PMMA films compared to those of the mononuclear complexes.<sup>37, 38</sup>

Table 1. Photophysical data for **1-4** in PMMA films and solid state in the air at 298K

C.	Media	$\lambda_{\text{exc}}$ (nm)	$\lambda_{\text{em}}$ (nm)	CIE (x;y)	$\tau$ ( $\mu\text{s}$ )	$\phi$ (%)	$k_r^b$	$k_{nr}^c$
<b>1</b>	PMMA <sup>a</sup>	390	483 <sub>max</sub> , 517 <sub>sh</sub> , 567 <sub>sh</sub>	0.18; 0.32	3.7	20	$5.4 \cdot 10^4$	$21.6 \cdot 10^4$
	PMMA <sup>a</sup>	350	483 <sub>max</sub> , 517 <sub>sh</sub> , 567 <sub>sh</sub>	0.18; 0.32		72		
	solid	390	469, 527 <sub>sh</sub> , 556 <sub>max</sub>	0.41; 0.52	0.4 (20%) 1.4 (80%)	3	$2.5 \cdot 10^4$	$79.2 \cdot 10^4$
<b>2</b>	PMMA <sup>a</sup>	390	469, 485 <sub>max</sub> , 524 <sub>sh</sub>	0.16; 0.29	3.5	54	$15.4 \cdot 10^4$	$13.1 \cdot 10^4$
	PMMA <sup>a</sup>	370	473, 492 <sub>max</sub> , 536 <sub>sh</sub>	0.16; 0.27		83		



	solid	390	472, 527 <sub>sh</sub> , 559 <sub>max</sub>	0.41; 0.53	0.3 (22%) 1.1 (78%)	3	3.2 10 <sup>4</sup>	103.2 10 <sup>4</sup>
<b>3</b>	PMMA <sup>a</sup>	390	464, 484 <sub>max</sub> , 523 <sub>sh</sub>	0.15; 0.25	3.4	53	15.7 10 <sup>4</sup>	13.8 10 <sup>4</sup>
	PMMA <sup>a</sup>	380	464, 484 <sub>max</sub> , 523 <sub>sh</sub>	0.15; 0.25		79		
	solid	390	468, 487 <sub>max</sub>	0.19; 0.35	0.3 (32%) 0.6 (68%)	16	30.1 10 <sup>4</sup>	158.1 10 <sup>4</sup>
	Grinded solid	390	468, 492 <sub>max</sub> , 519	0.29; 0.47	0.2 (20%) 0.6 (80%)	6	11.2 10 <sup>4</sup>	175.4 10 <sup>4</sup>
<b>4</b>	PMMA <sup>a</sup>	390	480 <sub>max</sub>	0.14; 0.26	2.2	69	31.7 10 <sup>4</sup>	14.1 10 <sup>4</sup>
	PMMA <sup>a</sup>	380	480 <sub>max</sub>	0.14; 0.26		86		
	solid	390	469, 482 <sub>max</sub> , 553 <sub>sh</sub>	0.24; 0.37	0.5 (30%) 1.1 (70%)	29	32.9 10 <sup>4</sup>	80.7 10 <sup>4</sup>
	Grinded solid	390	553 <sub>max</sub>	0.39; 0.55	1.1 (33%) 2.2 (67%)	51	28.3 10 <sup>4</sup>	27.2 10 <sup>4</sup>

<sup>a</sup> 5% wt; <sup>b</sup> Radiative decay rate constant given as  $k_r = \phi/\tau_{\text{exp}}$ ; <sup>c</sup>  $k_{nr} = (1-\phi)/\tau_{\text{exp}}$

Note that the large radiative rate constant values ( $kr$ , Table 1) support this. Also, compared to **2-4** ( $kr > 1.0 \times 10^5 \text{ s}^{-1}$ ), a smaller radiative rate constant was obtained for **1** ( $kr = 1.0 \times 10^4 \text{ s}^{-1}$ ), suggesting that the spin-orbit coupling (SOC) efficiency was lower because of a larger energy separation between the manifold of triplet and singlet states.<sup>44</sup> Exemplarily, from the absorption and the PMMA emission data, the energy differences between S<sub>1</sub> and T<sub>1</sub> ( $\Delta E_{S-T} = 0.93 \text{ eV } \mathbf{1}$ ,  $0.81 \text{ eV } \mathbf{2}$ ;  $0.75 \text{ eV } \mathbf{3}$ ,  $0.70 \text{ eV } \mathbf{4}$ ) were found to follow the same trend observed for the  $kr$ .

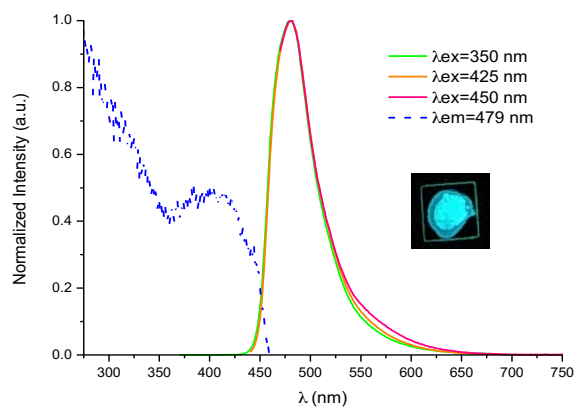
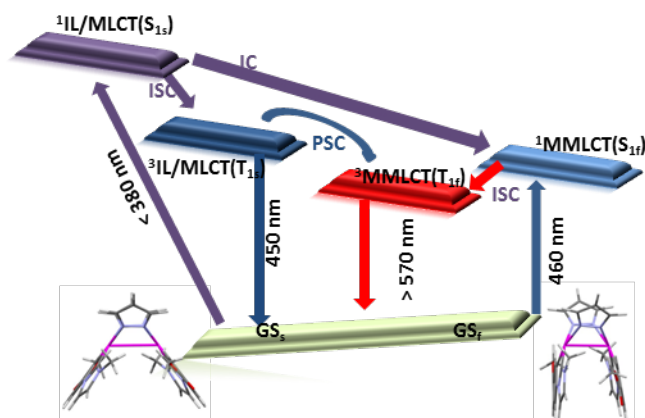


Figure 6: Normalized emission and excitation spectra of complex **4** in 5% wt PMMA film in the air; picture was taken under 365 nm UV light.

In solution at room temperature, compounds **1-4** are scarcely luminescent even in an argon atmosphere, an usual feature for blue-emitting Pt(II) complexes since population of  $dd^*$  states or formation of exciplexes are very common thermal quenching processes.<sup>43</sup> However, in fluid solution of 2-MeTHF ( $10^{-5}$  M) at r.t. under argon atmosphere (Figures S13 in SI), excitation in the low-energy absorption range ( $\lambda \leq 380$  nm), renders for complexes **1** and **2** a weak emission from **1s** and **2s**, for complex **3** a dual emission with maxima at 456 nm and 552 nm, likely corresponding to **3s** and **3f** and for complex **4** an emission with maximum at 559 nm arising from **4f**, according to theoretical calculations.

In summary, photoexcitation of complexes **1-4** at  $\lambda < 380$  nm allows the major **1s-4s** conformers to reach the high-energy  $^1IL/MLCT$  excited state; then, by a rapid intersystem crossing (ISC) the  $^3IL/MLCT$  ( $T_s$ ) state will be populated, that is calculated to have a similar Pt-Pt separation than the one of its corresponding ground state geometry (see scheme 2). In fluid solution, where the geometries of neither ground states nor those of the excited states are constrained, a photoinduced structural change (PSC) process between  $T_s$  and  $T_f$  conformers could happen

depending on both,  $\Delta G$  ( $T_f-T_s$ ) and the PSC energy barrier.<sup>28</sup> In the case of **4**, the computed barrierless PSC process along with the large  $\Delta G$  values ( $T_{4f}-T_{4s} = -0.166$  eV, -3.83 kcal) leads to  $T_{4f}$  almost in an exclusive manner. This piece of evidence explains why the emission from  $T_{4f}$  is the only one observed experimentally. In case of complex **3**, characterized by a smaller  $\Delta G$  ( $T_{3f}-T_{3s} = -0.84$  eV, -1.93 kcal) and a non-negligible PSC barrier (0.132 eV, 3.04 kcal), a thermal equilibrium between  $T_{3s}$  and  $T_{3f}$  is likely at r.t., and thus explaining its dual emission.



Scheme 2. Schematic diagrams of photophysical processes based on the steady-state excitation and emission spectra along with the results of the theoretical investigations

In the case of complex **2** with lower  $\Delta G$  ( $T_{2f}-T_{2s} = -0.015$  eV, -0.36 kcal), but larger energy barrier (0.162 eV, 3.73 kcal/mol) the PSC seems not to take place and the emission arises only from  $T_{2s}$ . For complex **1**, with  $\Delta G$  ( $T_{1f}/T_{1s} = 0.085$  eV, 1.95 kcal) and PSC energy barrier (0.115 eV, 2.65 kcal) on the same order of magnitude than those calculated for complex **3**, the PSC was expected to occur, but however, the emission arises only from  $T_{1s}$ .

In this case, we recently reported that internal conversion (IC) from  $^1\text{IL/MLCT}$  to  $^1\text{MMLCT}$  competes with ISC to  $^3\text{IL/MLCT}$ .<sup>33</sup> Therefore, a faster quenching of the  $^1/3\text{MMLCT}$  states of

complex **1**, as compared to that occurring in complexes **3** and **4**, enabled by the lack of steric hindrance of the reactive positions in complex **1**, could account for the absence of this low-energy emission.

In rigid media (2-MeTHF  $10^{-5}$  M at 77K or PMMA films), photoexcitation of complexes **1-4** at  $\lambda < 380$  nm leads in an analogous manner to the emission from the higher-lying triplet state  $^3\text{IL/MLCT}$ , despite the greater stability of the  $^3\text{MMLCT}$  state. This indicates that the energy barriers to connect the  $T_s/T_f$  wells are large enough to prevent the PSC in 2-MeTHF at 77K and it is also in agreement with PMMA being a rigid glass at r.t. ( $T_g = 378$  K).<sup>29</sup> Notably, the frozen glass environment leads to a deceleration of the nonradiative pathways and thus leading to large PLQY values in PMMA films (see Table 1).

On the other hand, irradiation at  $\lambda > 400$  nm will populate the low-energy states of the minor **1f-4f** conformers,  $^1\text{IL/MLCT}$  with some  $^1\text{MMLCT}$  character (see right panel in Scheme 2). A fast ISC to the close-lying triplet state  $^3\text{IL/MLCT}$ ,<sup>45</sup> would lead to the high-energy emission, which is the only one observed in 5% wt PMMA films of **1-4**. The low PLQYs when compared with those observed by irradiation at  $\lambda < 380$  nm (see Table S27 and Figure S12 in SI), are in agreement with the low ratio of butterfly-folded molecules in the samples, but still being significant. Therefore, for complexes **2-4**, the existence of close-lying  $^1\text{IL/MLCT/MMLCT}$ - $^3\text{IL/MLCT}$  states makes possible to get intense blue-emissions (PLQY: 40%-60%) from doped films by irradiation with wavelengths in the visible region.

**Mechanoluminescence in the solid state.** The as-prepared powders of **1** and **2** are scarcely emissive. They exhibit a weak (PLQY  $< 5\%$ ) broad structureless emission centered at  $\lambda \sim 555$  nm (Table 1 and Figure S14) with a shoulder at  $\lambda \sim 450$  nm. The shape and energy of the main band could match with the one arising from the low-lying triplet state for the butterfly-folded

molecules that is the  $^3\text{MMLCT}$  state. Yet, the role of excimeric  $^3\pi\text{-}\pi^*$  states can be not fully disregarded, given the extended and numerous intermolecular  $\pi\text{-}\pi$  interactions observed in the single-crystal X-ray structures of **1** and **2** (see Figure S6) and the lower quantum yield of compounds **1** and **2** in solid state compared to those in 5 % wt PMMA films. Keeping in mind that other mononuclear Pt(II) compounds containing cyclometalated NHCs reported previously<sup>42, 46, 47</sup> exhibit a similar behavior mainly as a consequence of  $\pi\text{-}\pi$  intermolecular interactions, it seems likely that the emission of **1** and **2** arises from excimeric  $^3\pi\text{-}\pi^*$  states with intermolecular  $\pi\text{-}\pi$  interactions affording efficient non-emissive deactivation channels<sup>12</sup> through an *aggregation-caused quenching* (ACQ) effect.<sup>9, 48</sup> Neither the excitation nor the emission spectra of **1** and **2** exhibit changes after grinding the solids with a mortar and pestle (see Figure S15 for **2** as example). However, complexes **3** and **4**, exhibit mechanoluminescence in the solid state. After grinding, the pale-yellow solids do not visually change their colours but their photoluminescence changes from blue to yellowish-green. Before to be grinded, a powdered sample of **3** exhibits a sky-blue emission, similar but weaker than that exhibited in PMMA film (5 % wt), which we attribute to  $^3\text{IL/MLCT}$ . After grinding, the emission becomes green (Figure S16) due to the presence of an intense lower-energy band with  $\lambda \sim 540$  nm, that could be assigned to the  $^3\text{MMLCT}$  state of molecules with butterfly-folded configuration in accordance with the theoretical calculations. However, in view of the intermolecular  $\pi\text{-}\pi$  interactions observed in the single-crystal X-ray structure of **3** (see Figure S6) and the decreased PLQY upon grinding, the participation of excimeric  $^3\pi\text{-}\pi^*$  states to the low-energy band cannot be ruled-out.<sup>9, 48</sup>

In case of compound **4**, photoexcitation of as-prepared powder leads to a greenish-blue emission with  $\lambda_{\text{max}}$  at 480 nm and an incipient shoulder at 553 nm, that can be assigned to  $^3\text{IL/MLCT}$  and  $^3\text{MMLCT}$  emissions respectively, in accordance with the theoretical calculations and with the

$^3\text{MMLCT}$  emission observed for  $[\{\text{Pt}(\text{C}^*\text{C}^*)(\mu\text{-NPh-CH-NPh})\}_2]$  exhibiting a short Pt...Pt distance, of about  $2.8 \text{ \AA}$ .<sup>24</sup> Mechanical grinding resulted in a suppression of the  $^3\text{IL/MLCT}$  band along with an increase of the  $^3\text{MMLCT}$  one and, unlike complex **3**, an enhancement of the PLQY (see Figure 7). As a result, the photoluminescence of powdery samples of **4** is intensified and changed from greenish-blue to yellowish-green upon grinding.

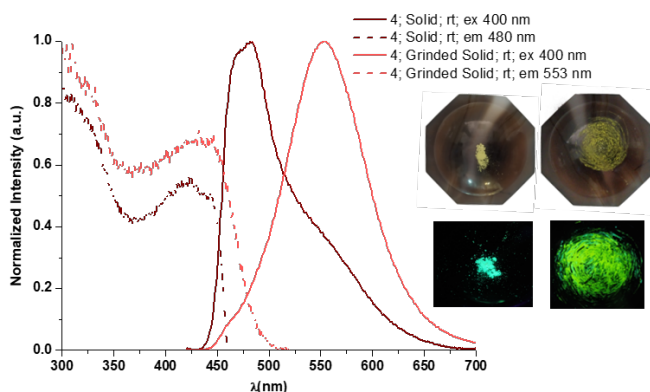


Figure 7. Normalized emission and excitation spectra of complex **4** in solid state in the air at room temperature; pictures were taken under 365 nm UV light

From the excitation and emission spectra it seems that the as-prepared powder of **4** shows phosphorescence from the two kind of conformers **4s** and **4f**, being that from **4s** the predominant. This is in agreement with the butterfly-spread conformer, **4s** being the major one in the GS and the fact that no PSC can take place in rigid media. Mechanical grinding seems to induce changes in the GS, that somehow shorten the Pt-Pt distances and enforces the intramolecular Pt-Pt interactions, in such a way that in the grinded solid, **4-g** the phosphorescence arises mainly from **4f**.

Structural changes involving the intramolecular Pt-Pt separation in the GS as the origin of mechanoluminescence seems plausible on the bases of experimental and theoretical data and once other causes were dismissed, like desolvation, since there is no solvent embedded in the solid (see CHN elemental analysis and NMR experiments) or intermolecular interactions, since we proved that the luminescence spectrum of **4** in 40wt% doped PMMA films match with that at 5wt% (see Figure S17) and its PLQY drops to 40%.

The grinded solid, **4-g** undergoes the reverse change partially upon cooling to 77K, as deduced from the emission and excitation spectra collected at r.t. and 77K (Figure S18).

Structural changes involving the intramolecular Pt-Pt separation in the GS were reported for the thermochromic platinum-butterfly compound  $[\{\text{Pt}(\text{ppy})(\mu\text{-Ph}_2\text{pz})\}_2]$ ,<sup>29</sup> but those induced by mechanical grinding have never been reported. In this case, like in complex **4** elongation of the Pt-Pt distance occurs when the temperature drops. Also, the transformations resulted to be reversible by addition of THF, toluene or diethyl ether to the grinded samples of **3** and **4** that led to the recovery of the blue emission (see Figure 8 and S19), and thus presumably restoring the previous structure arrangement.

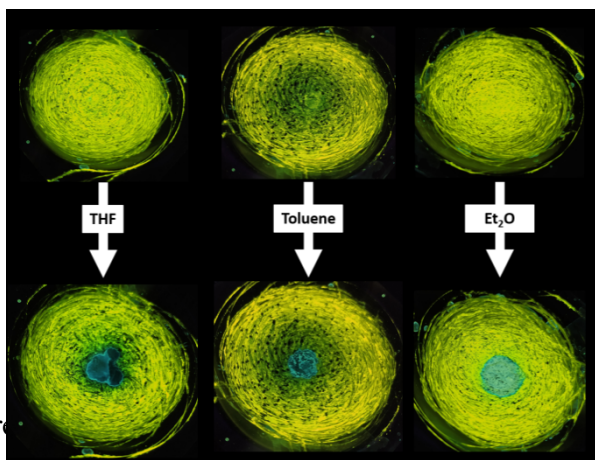


Figure 8. Reversible mechanoluminescence of grinded samples of **4** in response to solvent treatment taken under 365 nm-UV light

Therefore, it could be argued that the bulkiness of the  $\mu$ -pyrazolates has a strong impact not only on the luminescence, but also on the mechanoluminescence of these platinum butterflies in the solid state. As the bulkiness increases, the intermolecular  $\pi$ - $\pi$  interactions become more hindered, affording a less efficient non-emissive deactivation channels and consequently a more efficient emission. In addition, as the steric demand of the  $\mu$ -pyrazolates increases, the Pt-Pt interaction, enhanced by mechanical stimulation, causes a bathochromic shift of the emission ( $2750\text{ cm}^{-1}$  **4**) along with a remarkable increment of its PLQY.<sup>49-54</sup>

## CONCLUSIONS

Photoluminescence and DFT calculations on a new series of platinum-butterflies, [ $\{\text{Pt}(\text{C}^{\wedge}\text{C}^*) (\mu\text{-Rpz})\}_2$ ] (Rpz: pz **1**, 4-Mepz **2**, 3,5-dmpz **3**, 3,5-dppz **4**) containing a cyclometalated NHC in their wings, proof the presence of two conformers in the ground state at r.t., the butterfly-spread, **1s-4s** and the butterfly-folded, **1f-4f** ones, which are characterized by long and short Pt-Pt separations respectively. DFT calculations revealed that the former are the more stable in the GS but, in most of them, low  $\Delta G$  (s/f) and low energy barriers in solution of THF supports a fast thermal equilibration in the ground state PES, thus resembling an intramolecular *butterfly flapping-like* motion. By contrast, the butterfly-folded, **1f-4f** conformers, are the more stable in the  $T_1$  PES. In 5% wt doped PMMA films in the air, these complexes show intense sky-blue emissions (PLQY: 72.0% - 85.9%) upon excitation at  $\lambda \leq 380\text{ nm}$  mainly arising from a  $^3\text{IL/MLCT}$  excited state, the first triplet state of the major butterfly-spread conformer **1s-4s**, according with no PSC occurring in a rigid matrix. The existence of close-lying  $^1\text{IL/MLCT/MMLCT}$ -  $^3\text{IL/MLCT}$  states for the **1f-**



**4f** species enables to get intense blue-emissions (PLQY: 40%-60%) under excitation with wavelengths in the visible region, up to 450 nm.

In addition, it could be argued that the bulkiness of the  $\mu$ -pyrazolates has a strong impact on the luminescence and mechanoluminescence of these platinum butterflies in solid state. In complexes **3** and **4** the intermolecular  $\pi$ - $\pi$  interactions become more hindered than in complexes **1** and **2**, affording more efficient emissions. Besides, in the 3,5-dppz derivative, **4**, mechanical grinding causes a bathochromic shift of the emission from greenish-blue to yellowish-green along with a remarkable increment of its PLQY. This mechanoluminescence mechanism has been associated with an intramolecular structural change in the GS that somehow shortens the Pt-Pt distances and enhances the Pt-Pt interactions, in such a way that the thermal butterfly-flapping can be induced by mechanical grinding.

**KEYWORDS:** Platinum, dinuclear complexes, photoluminescence, mechanoluminescence, Pt·Pt interactions.

## **ASSOCIATED CONTENT**

### **Supporting Information.**

The Supporting Information is available free of charge at

General procedures and materials; crystallographic data; computational methods, NMR figures; description of single-crystal X-ray structures (CCDC: 2077779-2077780), DFT and PCM-DFT studies, Additional figures for the photophysical study.

## **AUTHOR INFORMATION**

### **Corresponding Authors**

**Violeta Sicilia**- *Departamento de Química Inorgánica, Escuela de Ingeniería y Arquitectura de Zaragoza, Instituto de Síntesis Química y Catálisis Homogénea (ISQCH), CSIC - Universidad de*

Zaragoza, Campus Rio Ebro, Edificio Torres Quevedo, 50018, Zaragoza (Spain).E-mail:

[sicilia@unizar.es](mailto:sicilia@unizar.es)

**Daniel Escudero**- Department of Chemistry, KU Leuven, Celestijnenlaan 200f - box 2404, 3001

Leuven. E-mail: [daniel.escudero@kuleuven.be](mailto:daniel.escudero@kuleuven.be)

**Sara Fuertes**- Departamento de Química Inorganica,, Facultad de Ciencias, Instituto de Síntesis Química y Catalisis Homogenea (ISQCH), CSIC - Universidad de Zaragoza, Pedro Cerbuna 12, 50009, Zaragoza (Spain)

### Authors

**Lorenzo Arnal**- Departamento de Química Inorganica,, Facultad de Ciencias, Instituto de Síntesis Química y Catalisis Homogenea (ISQCH), CSIC - Universidad de Zaragoza, Pedro Cerbuna 12, 50009, Zaragoza (Spain)

**Antonio Martin**- Departamento de Química Inorganica,, Facultad de Ciencias, Instituto de Síntesis Química y Catalisis Homogenea (ISQCH), CSIC - Universidad de Zaragoza, Pedro Cerbuna 12, 50009, Zaragoza (Spain)

### Author Contributions

The manuscript was written through contributions of all authors. All authors have given approval to the final version of the manuscript.

### Funding Sources

This work was supported by the Spanish Ministerio de Economía y Competitividad (Ministerio de Ciencia Innovación y Universidades)/FEDER (Project PGC2018-094749-B-I00), by the Gobierno de Aragón (Grupo E17\_20R: Química Inorgánica y de los Compuestos Organometálicos) and by Internal Funds KU Leuven

### Notes

The authors declare no competing financial interest.

## ACKNOWLEDGMENT

This work was supported by the Spanish Ministerio de Economía y Competitividad (Ministerio de Ciencia Innovación y Universidades)/FEDER (Project PGC2018-094749-B-I00), by the Gobierno de Aragón (Grupo E17\_20R: Química Inorgánica y de los Compuestos Organometálicos) and by Internal Funds KU Leuven. L. A. acknowledges the support of a grant from the Gobierno de Aragón.

## REFERENCES

1. Herberger, J.; Winter, R. F., Platinum Emitters with Dye-Based *r*-Aryl Ligands. *Coord. Chem. Rev.* **2019**, *400*, 213048.
2. Shigeta, Y.; Kobayashi, A.; Yoshida, M.; Kato, M., Stability Tuning of Vapor-Adsorbed State of Vapochromic Pt(II) Complex by Introduction of Chiral Moiety. *Inorg. Chem.* **2019**, *58*, 7385- 7392.
3. Law, A. S. Y.; Lee, L. C. C.; Yeung, M. C. L.; Lo, K. K. W.; Yam, V. W. W., Amyloid Protein-Induced Supramolecular Self-Assembly of Water-Soluble Platinum(II) Complexes: A Luminescence Assay for Amyloid Fibrillation Detection and Inhibitor Screening. *J. Am. Chem. Soc.* **2019**, *141*, 18570-18577.
4. Liao, J. L.; Chi, Y.; Wang, J. Y.; Chen, Z. N.; Tsai, Z. H.; Hung, W. Y.; Tseng, M. R.; Lee, G. H., Pt(II) Phosphors Featuring Both Dicarbene and Functional Biazolate Chelates: Synthesis, Luminescent Properties, and Applications in Organic Light-Emitting Diodes. *Inorg. Chem.* **2016**, *55*, 6394-6404.

5. Pinter, P.; Strassner, T., Prediction of the Efficiency of Phosphorescent Emitters: A Theoretical Analysis of Triplet States in Platinum Blue Emitters. *Chem. Eur. J.* **2019**, *25*, 4202-4205.
6. Sukpattanacharoen, C.; Kumar, P.; Chi, Y.; Kungwan, N.; Escudero, D., Formation of Excimers in Isoquinolinyll Pyrazolate Pt(II) Complexes: Role of Cooperativity Effects. *Inorg. Chem.* **2020**, *59*, 18253-18263.
7. Fornies, J.; Sicilia, V.; Borja, P.; Casas, J. M.; Diez, A.; Lalinde, E.; Larraz, C.; Martin, A.; Moreno, M. T., Luminescent Benzoquinolate-Isocyanide platinum(II) Complexes: Effect of Pt··Pt and  $\pi$ - $\pi$  Interactions on their Photophysical properties. *Chem. Asian J.* **2012**, *7*, 2813-2823.
8. Saito, D.; Ogawa, T.; Yoshida, M.; Takayama, J.; Hiura, S.; Murayama, A.; Kobayashi, A.; Kato, M., Intense Red-Blue Luminescence Based on Superfine Control of Metal-Metal Interactions for Self-Assembled Platinum(II) Complexes. *Angew. Chem. Int. Ed.* **2020**, *59*, 18723-18730.
9. Le Bras, L.; Chaitou, K.; Aloise, S.; Adamo, C.; Perrier, A., Aggregation-Caused Quenching versus Crystallization Induced Emission in thiazolo[5,4-b]thieno[3,2-e]-pyridine (TTP) Derivatives: Theoretical Insights. *Phys.Chem.Chem.Phys.* **2019**, *21*, 46-56.
10. Alam, P.; Climent, C.; Alemany, P.; Laskar, R., "Aggregation-Induced Emission" of Transition Metal Compounds: Design, Mechanistic Insights and Applications. *J. Photochem. photobiol. C* **2019**, *41*, 100317.

11. Zhu, S.; Hu, J.; Zhai, S.; Wang, Y.; Xu, Z.; Liu, R.; Zhu, H., AIPE-Active Pt(II) Complexes with a Tunable Triplet Excited State: Design, Mechanochromism and Application in Anti-Counterfeiting. *Inorg. Chem. Front.* **2020**, *7*, 4677-4686.
12. Martinez-Junquera, M.; Lara, R.; Lalinde, E.; Moreno, M. T., Isomerism, Aggregation-Induced Emission and Mechanochromism of Isocyanide Cycloplatinated(II) Complexes. *J. Mater. Chem. C* **2020**, *8*, 7221-7233.
13. Pinter, P.; Pittkowski, R.; Soellner, J.; Strassner, T., The Chameleonic Nature of Platinum(II) Imidazopyridine Complexes. *Chem. Eur. J.* **2017**, *23*, 14173 – 14176.
14. Pinter, P.; Mangold, H.; Stengel, I.; Münster, I.; Strassner, T., Enhanced Photoluminescence Quantum Yields through Excimer Formation of Cyclometalated Platinum(II) N-Heterocyclic Carbene Complexes. *Organometallics* **2016**, *35*, 673–680.
15. Li, G.; Fleetham, T.; Li, J., Efficient and Stable White Organic Light-Emitting Diodes Employing a Single Emitter. *Adv. Mater* **2014**, *26*, 2931-2936.
16. Fleetham, T.; Li, J., Recent Advances in White Organic Light-Emitting Diodes Employing a Single-Emissive Material. *Journal of Photonics for Energy* **2014**, *4*, 040991-1-17.
17. Shafikov, M. Z.; Pander, P.; Zaytsev, A. V.; Daniels, R.; Martinscroft, R.; Dias, F. B.; Williams, J. A. G.; Kozhevnikov, V. N., Extended Ligand Conjugation and Dinuclearity as a Route to Efficient Platinum-based Near-Infrared (NIR) Triplet Emitters and Solution-Processed NIR-OLEDs. *J. Mater. Chem. C* **2021**, *9*, 127-135.
18. Nisic, F.; Colombo, A.; Dragonetti, C.; Roberto, D.; Valore, A.; Malicka, J. M.; Cocchi, M.; Freeman, G. R.; Williams, J. A. G., Platinum(II) Complexes with Cyclometallated

5- $\pi$ -Delocalized-Donor-1,3-di(2-pyridyl)benzene Ligands as Efficient Phosphors for NIR-OLEDs. *J. Mater. Chem. C* **2014**, *2*, 1791-1800.

19. Liu, L.; Wang, X.; Wang, N.; Peng, T.; Wang, S., Bright, Multi-responsive, Sky-Blue Platinum(II) Phosphors Based on a Tetradentate Chelating Framework. *Angew. Chem.* **2017**, *129*, 9288-9292.

20. Fornies, J.; Fuertes, S.; Lopez, J. A.; Martin, A.; Sicilia, V., New Water Soluble and Luminescent Platinum(II) Compounds, Vapochromic Behavior of  $[K(H_2O)][Pt(bzq)(CN)_2]$ , New Examples of the Influence of the Counterion on the Photophysical Properties of d8 Square-Planar Complexes. *Inorg. Chem.* **2008**, *47*, 7166-7176.

21. Puttock, E. V.; Walden, M. T.; Williams, J. A. G., The Luminescence Properties of Multinuclear Platinum Complexes. *Coord. Chem. Rev.* **2018**, *367*, 127-162.

22. Zhang, Q. C.; Xiao, H.; Zhang, X.; Xu, L. J.; Chen, Z. N., Luminescent Oligonuclear Metal Complexes and the Use in Organic Light-Emitting Diodes. *Coord. Chem. Rev.* **2019**, *378*, 121-133.

23. Chaaban, M.; Zhou, C.; Lin, H.; Chyi, B.; Ma, B., Platinum(II) Binuclear Complexes: Molecular Structures, Photophysical Properties, and Applications. *J. Mater. Chem. C* **2019**, *7*, 5910-5924.

24. Leopold, H.; Tenne, M.; Tronnier, A.; Metz, S.; Munster, I.; Wagenblast, G.; Strassner, T., Binuclear C<sup>^</sup>C\* Cyclometalated Platinum(II) NHC Complexes with Bridging Amidinate Ligands. *Angew. Chem. Int. Ed.* **2016**, *55*, 15779–15782.

25. Brown-Xu, S. E.; Kelley, M. S. J.; Fransted, K. A.; Chalcrabarty, A.; Schatz, G. C.; Castellano, F. N.; Chen, L. X., Tunable Excited-State Properties and Dynamics as a Function of Pt-Pt Distance in Pyrazolate-Bridged Pt(II) Dimers. *J. Phys. Chem. A* **2016**, *120* (4), 543-550.
26. Ma, B.; Li, J.; Djurovich, P. I.; Yousufuddin, M.; Bau, R.; Thompson, M. E., Synthetic Control of Pt··Pt Separation and Photophysics of Binuclear Platinum Complexes. *J. Am. Chem. Soc.* **2005**, *127*, 28-29.
27. Ma, B.; Djurovich, P. I.; Garon, S.; Alleyne, B.; Thompson, M. E., Platinum Binuclear Complexes as Phosphorescent Dopants for Monochromatic and White Organic Light-Emitting diodes. *Adv. Funct. Mater.* **2006**, *16*, 2438-2446.
28. Zhou, C.; Tian, Y.; Yuan, Z.; Han, M.; Wang, J.; Zhu, L.; Tameh, M. S.; Huang, C.; Ma, B., Precise Design of Phosphorescent Molecular Butterflies with Tunable Photoinduced Structural Change and dual Emission. *Angew. Chem. Int. Ed.* **2015**, *54*, 9591-9595.
29. Rachford, A. A.; Castellano, F. N., Thermochromic Absorption and Photoluminescence in  $[\{\text{Pt}(\text{ppy})(\mu\text{-Ph}_2\text{pz})\}_2]$  *Inorg. Chem.* **2009**, *48*, 10865-10867.
30. Chakraborty, A.; Deaton, J. C.; Haeefe, A.; Castellano, F. N., Charge-Transfer and Ligand-Localized Photophysics in Luminescent Cyclometalated Pyrazolate-Bridged Dinuclear Platinum(II) Complexes. *Organometallics* **2013**, *32*, 3819-3829.
31. Pinter, P.; Unger, Y.; Strassner, T., Cyclometalated NHC Platinum(II) Complexes with Bridging Pyrazolates: Enhanced Photophysics of Binuclear Blue Emitters. *ChemPhotoChem* **2017**, *1*, 113-115.
32. Pinter, P.; Soellner, J.; Strassner, T., Photophysical Properties of Phosphorescent Mono- and Bimetallic Platinum(II) Complexes with C<sup>^</sup>C\* Cyclometalating NHC Ligands. *Organometallics* **2021**, *40*, 557-563.

33. Sicilia, V.; Arnal, L.; Fuertes, S.; Martin, A.; Baya, M., Metal–Metal Cooperation in the Oxidation of a Flapping Platinum Butterfly by Haloforms: Experimental and Theoretical Evidence. *Inorg. Chem.* **2020**, *59*, 12586-12594.
34. Fuertes, S.; Chueca, A. J.; Peralvarez, M.; Borja, P.; Torrell, M.; Carreras, J.; Sicilia, V., White Light Emission from Planar Remote Phosphor Based on NHC Cycloplatinated Complexes. *ACS Appl. Mater. Interfaces* **2016**, *8*, 16160–16169.
35. Arnal, L.; Fuertes, S.; Martin, A.; Sicilia, V., The Use of Cyclometalated NHCs and Pyrazoles for the Development of Fully Efficient Blue Pt<sup>II</sup> Emitters and Pt/Ag Clusters. *Chem. Eur. J.* **2018**, *24*, 9377-9384.
36. Arnal, L.; Fuertes, S.; Martin, A.; Baya, M.; Sicilia, V., A Cyclometalated N-Heterocyclic Carbene: The Wings of the First Pt<sub>2</sub>(II,II) Butterfly Oxidized by CHI<sub>3</sub>. *Chem. Eur. J.* **2018**, *24*, 18743-18748.
37. Akatsu, S.; Kanematsu, Y.; Kurihara, T.-A.; Sueyoshi, S.; Arikawa, Y.; Onishi, M.; Ishizaka, S.; Kitamura, N.; Nakao, Y.; Sakaki, S.; Umakoshi, K., Syntheses and Luminescent Properties of 3,5-Diphenylpyrazolato-Bridged Heteropolynuclear Platinum Complexes. The Influence of Chloride Ligands on the Emission Energy Revealed by the Systematic Replacement of Chloride Ligands by 3,5-Dimethylpyrazolate. *Inorg. Chem.* **2012**, *51*, 7977-7992.
38. Umakoshi, K.; Kimura, K.; Kim, Y. H.; Tsukimoto, Y.; Arikawa, Y.; Onishi, M.; Ishizaka, S.; Kitamura, N., Pyrazolato- and 3,5-Dimethylpyrazolato-Bridged Dinuclear Platinum(II), Palladium(II), and Their Mixed-Metal Complexes of 2,2'-Bipyrimidine. Syntheses, Structures, and Luminescent Properties. *Bull. Chem. Soc. Jpn.* **2010**, *83*, 1504–1510



39. Ghavale, N.; Wadawale, A.; Dey, S.; Jain, V. K., Synthesis, Structures and Spectroscopic Properties of Platinum Complexes Containing Orthometalated 2-Phenylpyridine. *J. Organomet. Chem.* **2010**, *695*, 1237-1245.
40. Moon, S.; Horiuchi, S.; Sakuda, E.; Ito, A.; Arikawa, Y.; Umakoshi, K., Synthesis and Photophysical Properties of Butterfly-Shaped Dinuclear Pt(II) Complex Having NHC-Based Chelate Ligands. *Inorg. Chim. Acta* **2019**, *493*, 43-48.
41. Saito, K.; Nakao, y.; Sakai, S., Theoretical Study of Pyrazolate-Bridged Dinuclear Platinum(II) Complexes: Interesting Potential Energy Curve of the Lowest Energy Triplet Excited State and Phosphorescence Spectra. *Inorg. chem.* **2008**, *47*, 4329-4337.
42. Sicilia, V.; Fuertes, S.; Chueca, A. J.; Arnal, L.; Martin, A.; Peralvarez, M.; Botta, C.; Giovanella, U., Highly Efficient Platinum-Based Emitters for Warm White Light Emitting Diodes. *J. Mater. Chem. C* **2019**, *7*, 4509-4516.
43. Fuertes, S.; Chueca, A. J.; Martin, A.; Sicilia, V., New NHC Cycloplatinated Compounds. Significance of the Cyclometalated Group on the Electronic and Emitting Properties of Biscyanide Compounds. *J. Organomet. Chem.* **2019**, *889*, 53-61.
44. Ogawa, T.; Sameera, W. M. C.; Saito, D.; Yoshida, M.; Kobayashi, A.; Kato, M., Phosphorescence Properties of Discrete Platinum(II) Complex Anions Bearing N-Heterocyclic Carbenes in the Solid State. *Inorg.Chem.* **2018**, *57* (22), 14086-14096.
45. Kim, P.; Kelley, M. S.; Chakraborty, A.; Wong, N. L.; Van Duyne, R. P.; Schatz, G. C.; Castellano, F. N.; Chen, L. X., Coherent Vibrational Wavepacket Dynamics in Platinum(II) Dimers and Their Implications. *J. Phys. Chem. C* **2018**, *122*, 14195-14204.

46. Jaime, S.; Arnal, L.; Sicilia, V.; Fuertes, S., Cyclometalated NHCs Pt(II) Compounds with Chelating P<sup>^</sup>P and S<sup>^</sup>S Ligands: From Blue to White Luminescence. *Organometallics* **2020**, *39*, 3695-3704.
47. Sicilia, V.; Arnal, L.; Chueca, A. J.; Fuertes, S.; Babaei, A.; Igual Muñoz, A. M.; Sessolo, M.; Bolink, H. J., Highly Photoluminescent Blue Ionic Platinum-Based Emitters. *Inorg. Chem.* **2020**, *59*, 1145-1152.
48. Zhao, Z.; Zhang, H.; Lam, J. W. Y.; Tang, B. Z., Aggregation-Induced Emission: New Vistas at the Aggregate Level. *Angew. Chem. Int. Ed.* **2020**, *59*, 9888-9907.
49. Ku, H.-Y.; Tong, B.; Chi, Y.; Kao, H.-C.; Yeh, C.-C.; Chang, C.-H.; Lee, G.-H., Luminescent Pt(II) Complexes Bearing Dual Isoquinoliny Pyrazolates: Fundamentals and Applications. *Dalton Trans.* **2015**, *44* (18), 8552-8563.
50. Ni, J.; Wang, Y.-G.; Wang, H. i.-H.; Xu, L.; Zhao, Y.-Q.; Pan, Y.-Z.; Zhang, J.-J., Thermo- and Mechanical-Grinding-Triggered Color and Luminescence Switches of the Diimine-Platinum(II) Complex with 4-bromo-2,2'-bipyridine. *Dalton Trans.* **2014**, *43* (1), 352-360.
51. Zhang, X.; Zhang, L.-Y.; Wang, J.-Y.; Dai, F.-R.; Chen, Z.-N., Two-Step Phosphorescent Mechanochromism Due to Intramolecular Deformation. *J. Mater. Chem. C* **2020**, *8* (2), 715-720.
52. Genovese, D.; Aliprandi, A.; Prasetyanto, E. A.; Mauro, M.; Hirtz, M.; Fuchs, H.; Fujita, Y.; Uji-I, H.; Lebedkin, S.; Kappes, M.; De Cola, L., Mechano- and Photochromism from Bulk to Nanoscale: Data Storage on Individual Self-Assembled Ribbons. *Adv. Funct. Mater.* **2016**, *26* (29), 5271-5278.

53. Ni, J.; Zhang, X.; Qiu, N.; Wu, Y.-H.; Zhang, L.-Y.; Zhang, J.-J.; Chen, Z.-N.,  
Mechanochromic Luminescence Switch of Platinum(II) Complexes with 5-  
Trimethylsilylethynyl-2,2'-bipyridine. *Inorg. Chem.* **2011**, *50* (18), 9090-9096.
54. Han, A.; Du, P.; Sun, Z.; Wu, H.; Jia, H.; Zhang, R.; Liang, Z.; Cao, R.; Eisenberg,  
R., Reversible Mechanochromic Luminescence at Room Temperature in Cationic Platinum(II)  
Terpyridyl Complexes. *Inorg. Chem.* **2014**, *53* (7), 3338-3344.

## SYNOPSIS

The intriguing luminescence of a new series of platinum-butterfly molecules,  $[\{\text{Pt}(\text{C}^*\text{C}^*)(\mu\text{-Rpz})\}_2]$  have been studied and deciphered with DFT and TD-DFT calculations. The low energy barrier for the thermal interconversion between the spread (**4s**) and folded (**4f**) structures in the GS of the 3,5-diphenylpyrazolate compound, **4** seems to be as the basis of the stimuli-responsive luminescence of complex **4**.

